APPENDIX A

A_i & B_i combined represents six anisotropic constants where i = 1 to 3. Assuming material anisotropy to be orthogonal these constants are related to normal $(\sigma_{Y1}, \sigma_{Y2}, \sigma_{Y3})$ & shear yield stresses $(\tau_{Y12}, \tau_{Y23}, \tau_{Y31})$ (with respect to axis of anisotropy) respectively through the following relation.

$$A_1 = \frac{1}{2}\left\{\frac{1}{(\sigma_2^y)^2} + \frac{1}{(\sigma_3^y)^2} - \frac{1}{(\sigma_1^y)^2}\right\} \quad ; \quad B_1 = \frac{1}{2(\tau_{23}^y)^2}$$

$$A_2 = \frac{1}{2}\left\{\frac{1}{(\sigma_3^y)^2} + \frac{1}{(\sigma_1^y)^2} - \frac{1}{(\sigma_2^y)^2}\right\} \quad ; \quad B_2 = \frac{1}{2(\tau_{31}^y)^2}$$

$$A_3 = \frac{1}{2}\left\{\frac{1}{(\sigma_1^y)^2} + \frac{1}{(\sigma_2^y)^2} - \frac{1}{(\sigma_3^y)^2}\right\} \quad ; \quad B_3 = \frac{1}{2(\tau_{12}^y)^2}$$

- $when\ A_1 = 0\ then\ \sigma_{Y1} = \frac{\sigma_{Y2}\sigma_{Y3}}{\sqrt{(\sigma_{Y2})^2 + (\sigma_{Y3})^2}}\ ;\ if\ A_2 = 0\ then\ \sigma_{Y2} = \frac{\sigma_{Y3}\sigma_{Y1}}{\sqrt{(\sigma_{Y3})^2 + (\sigma_{Y1})^2}}$

  $and\ if\ A_3 = 0\ then\ \sigma_{Y3} = \frac{\sigma_{Y1}\sigma_{Y2}}{\sqrt{(\sigma_{Y1})^2 + (\sigma_{Y2})^2}}$
- $when\ B_1 = 0\ then\ \tau_{23}^y \rightarrow \infty\ ;\ if\ B_2 = 0\ then\ \tau_{31}^y \rightarrow \infty\ and\ if\ B_3 = 0\ then\ \tau_{12}^y \rightarrow \infty$
- $when\ A_1 = A_2\ then\ \sigma_1^y = \sigma_2^y\ ;\ if\ A_2 = A_3\ then\ \sigma_2^y = \sigma_3^y\ and\ if\ A_3 = A_1\ then\ \sigma_3^y = \sigma_1^y$

APPENDIX B

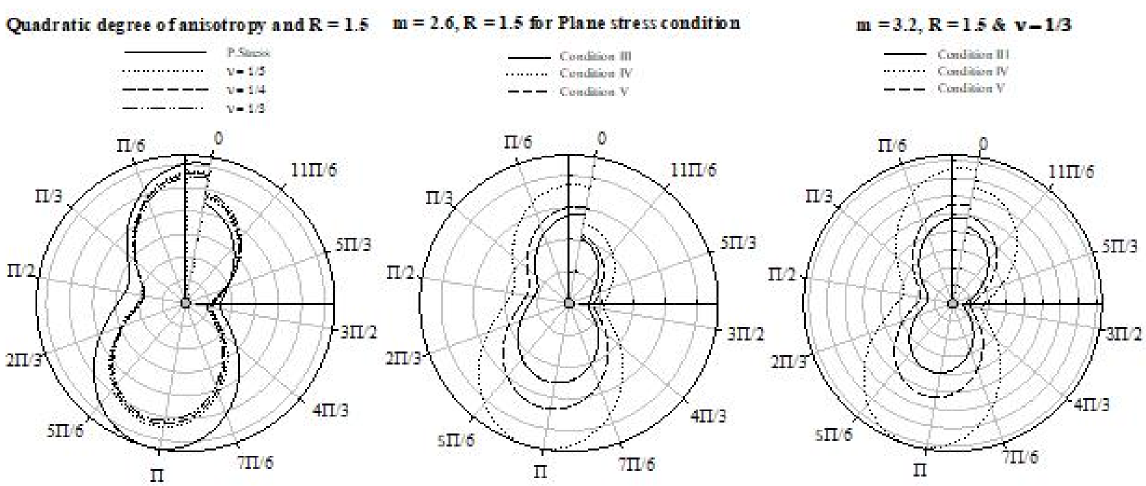

Fig 1 Comparison of Plastic zones at the crack tip for crack inclination 10°

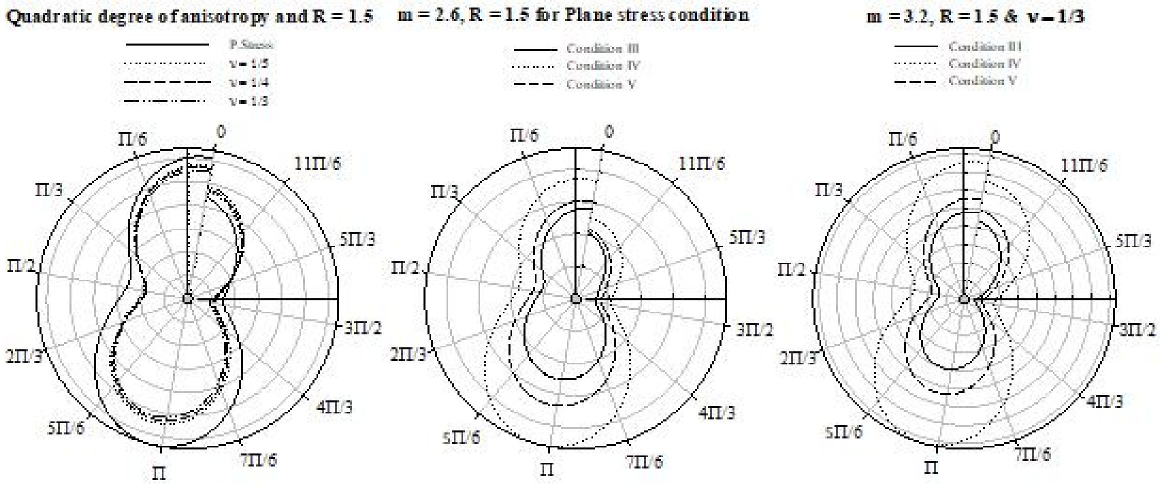

Fig 2 Comparison of Plastic zones at the crack tip for crack inclination 20˚

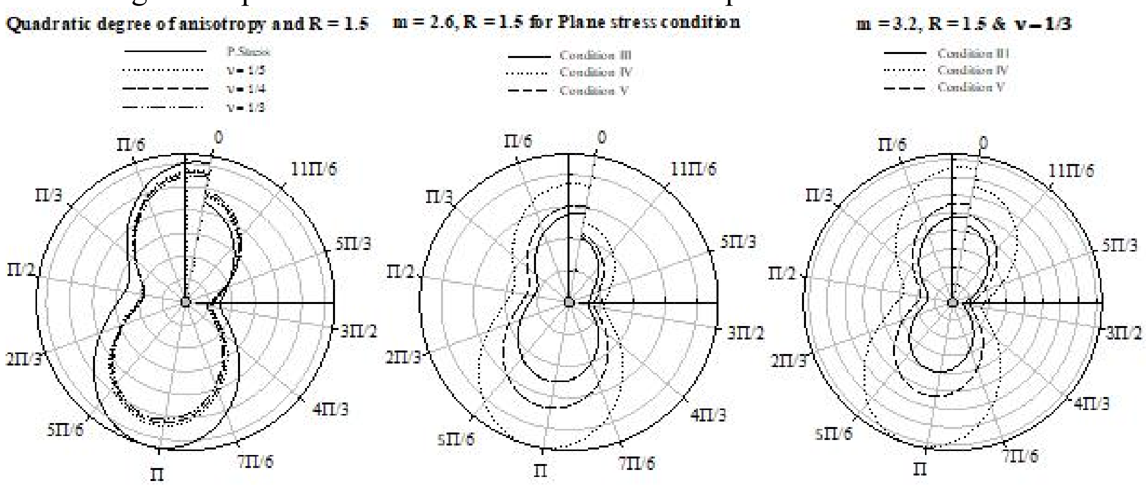

Fig 3 Comparison of Plastic zones at the crack tip for crack inclination 40˚

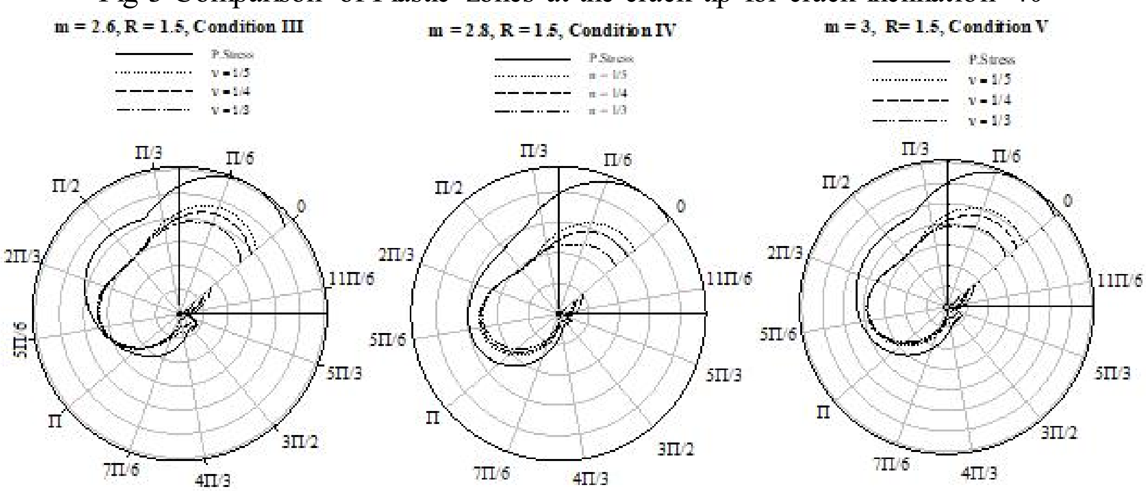

Fig 4 Comparison of Plastic zones at the crack tip for crack inclination 50˚

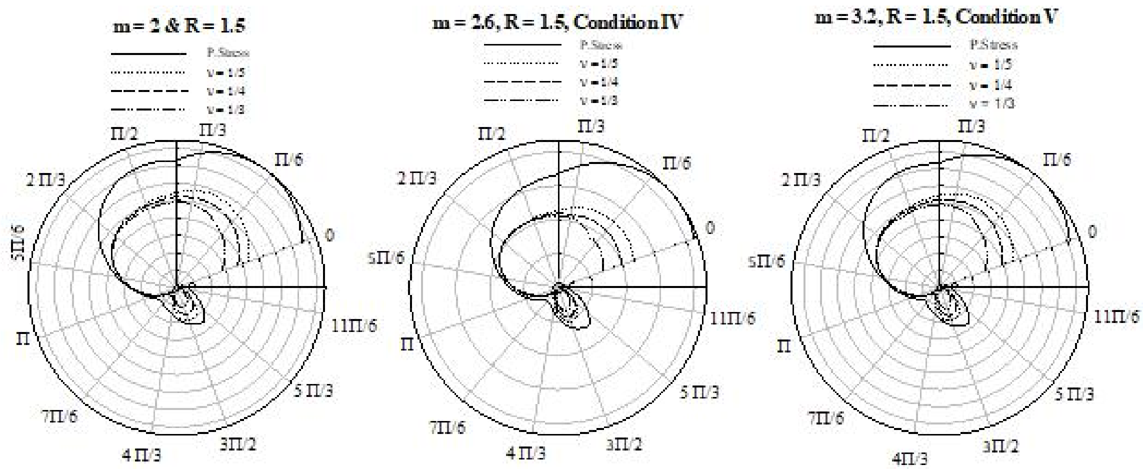

Fig 5.Comparison of Plastic zones at the crack tip for crack inclination 70˚

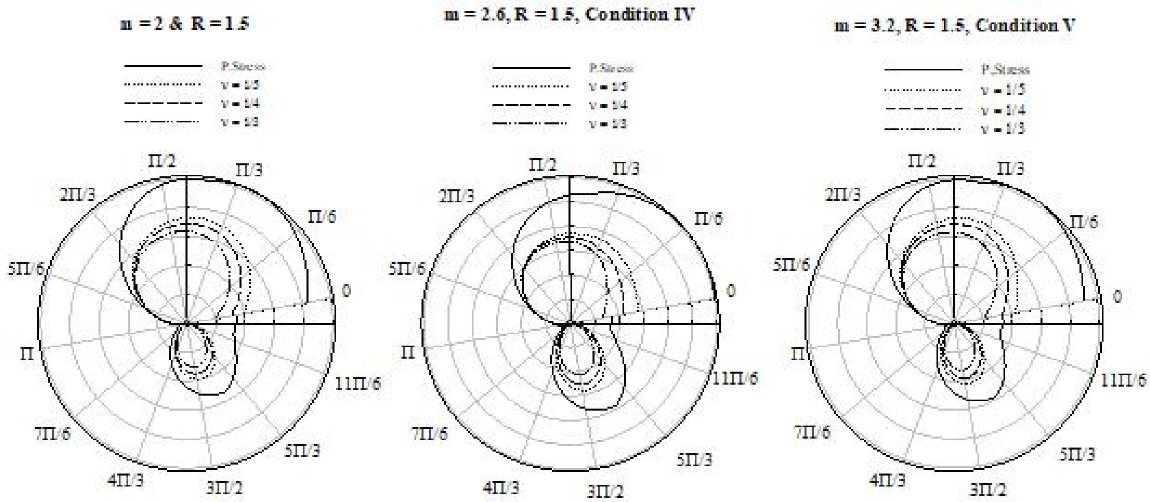

Fig 6.Comparison of Plastic zones at the crack tip for crack inclination 80˚

APPENDIX C

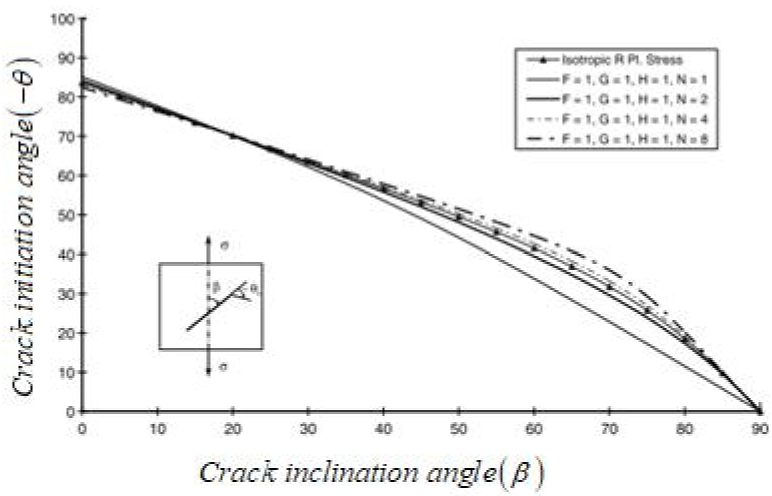

(a)

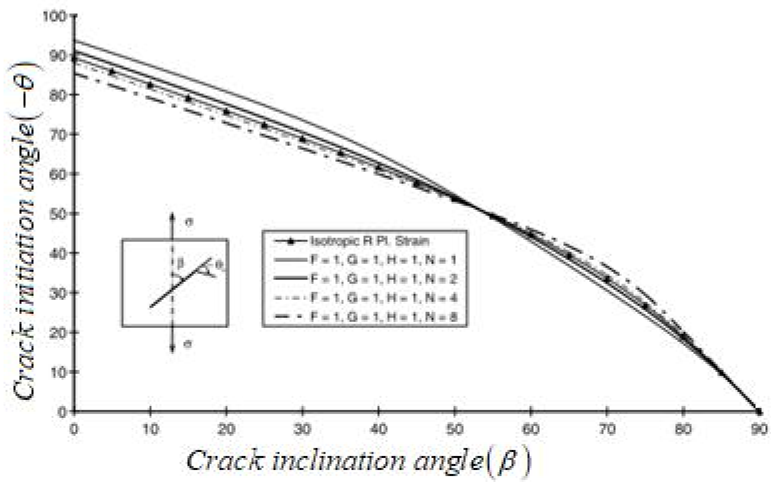

(b)

Fig 1 Effect of anisotropic constant (*N)* on crack initiation angle for uniaxial tension for (a) plane stress and (b) plane strain condition

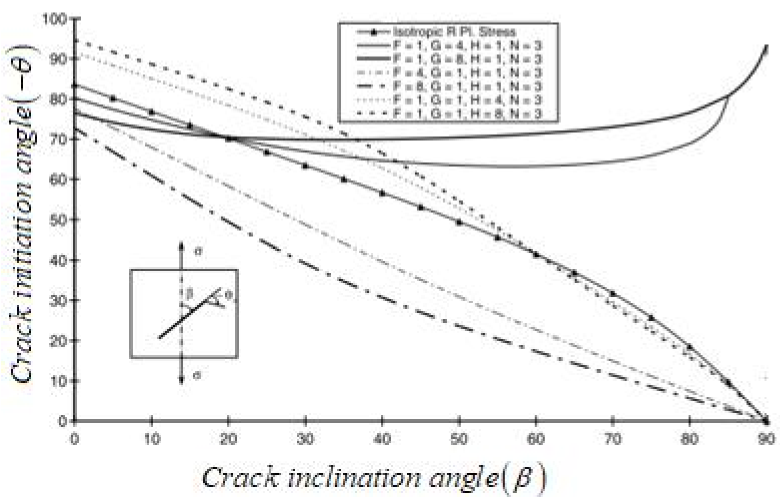

(a)

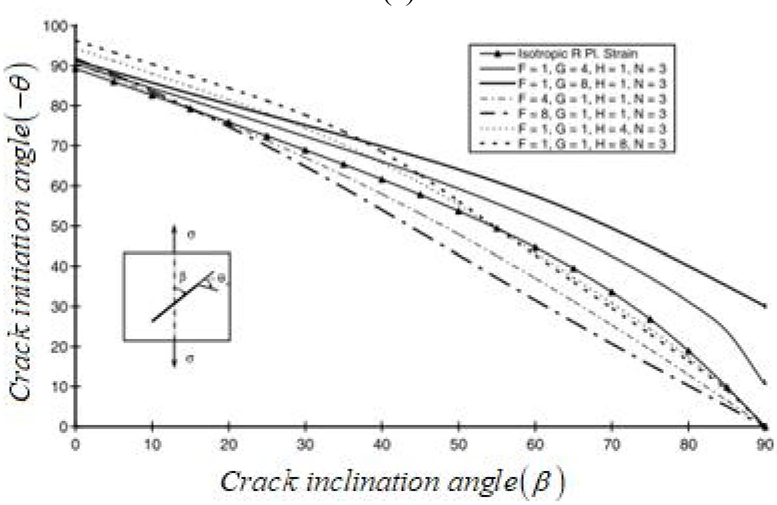

(b)

Fig 2 Effect of anisotropic constants (*F,G,H)* on crack initiation angles for uniaxial tension for (a) plane stress and (b) plane strain

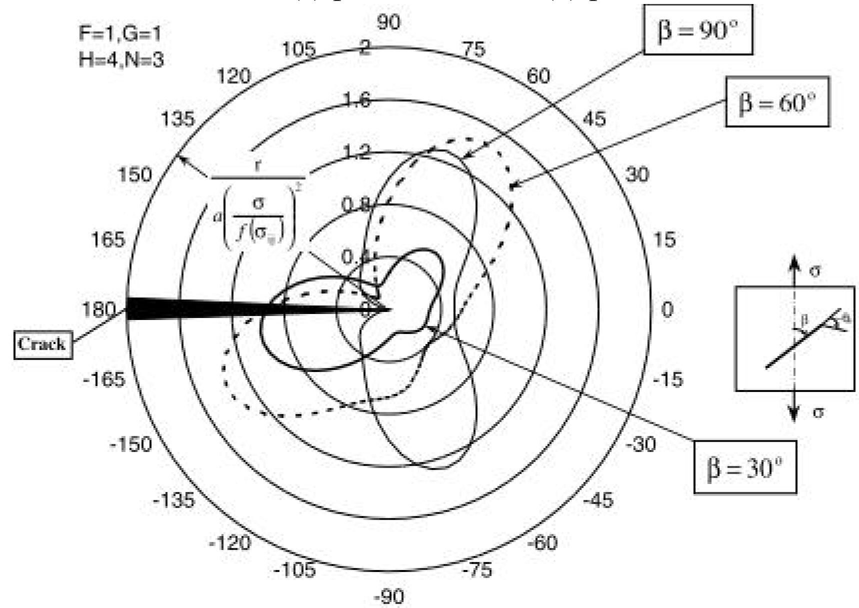

(a)

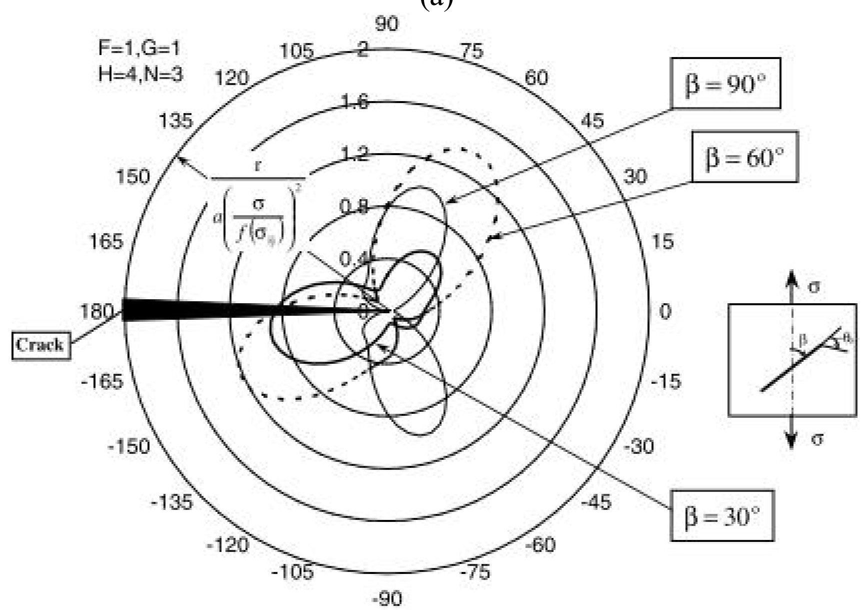

(b)

Fig 3 Effects of anisotropic constants (*F=1, G =1, H =4, N = 3*) on elastic–plastic core region (crack inclination 30˚, 60˚ & 90˚) under uniaxial tension for (a) plane stress and (b) plane strain

APPENDIX D

Figure 1 shows the meshed 2D numerical model of rectangular sheet (dimensions 200 x 100 mm) containing a central crack (of 10 mm length and 0.2 mm breadth) at the center of the sheet at various angles, for the calculation of crack initiation angle. The material taken into consideration is steel having Young's modulus of 2x1011 N/mm2 having Poisson’s ratio of 0.3. The element type for meshing is plane stress 182.

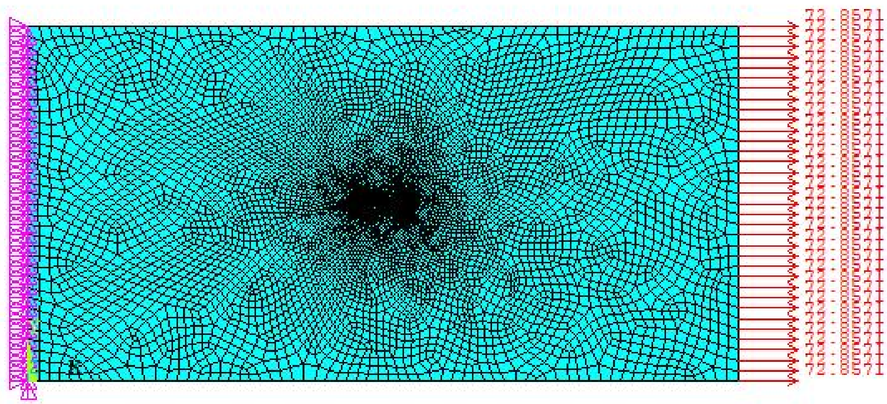

Fig 1 Meshing at the crack tip

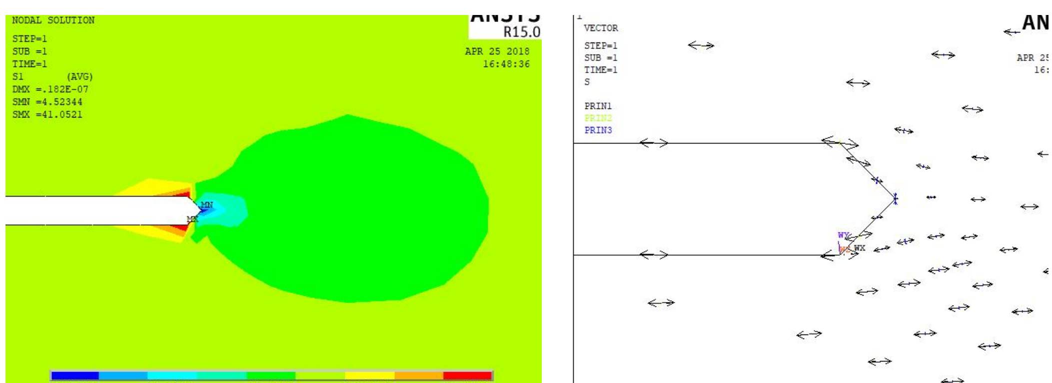

(a) (b)

Fig 2 (a) Stress contours at the crack tip and (b) Vector direction of various nodes at the crack tip inclined at 0° to the loading axis

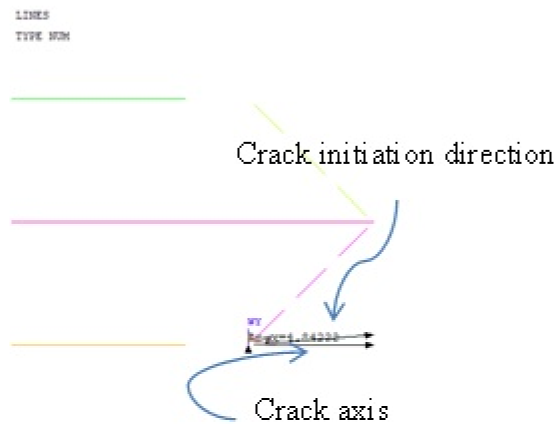

Fig 3 Vector direction of a node having maximum first principal stress (crack initiation angle) at the crack tip inclined at 0° to the loading axis

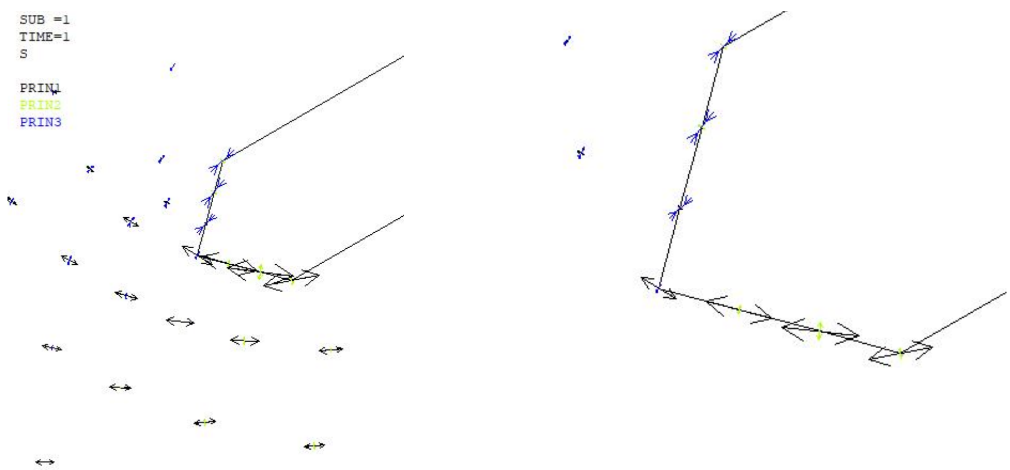

Fig 4 Vector direction of various nodes at and around the crack tip inclined at 30° to the loading axis

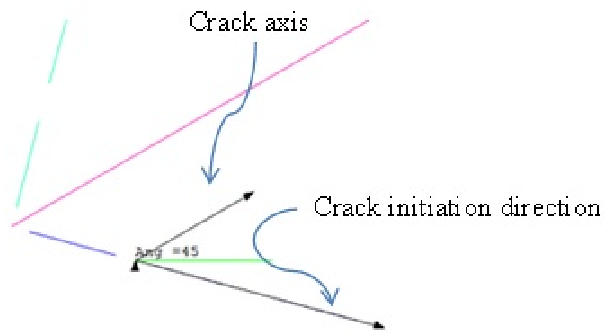

Fig 5 Vector direction of a node having maximum first principal stress for crack inclined at 30° to the loading axis

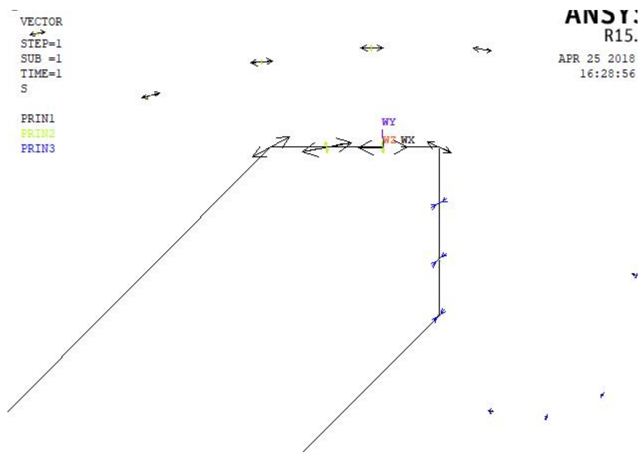

Fig 6 Vector direction of various nodes at and around the crack tip inclined at 45° to the loading axis

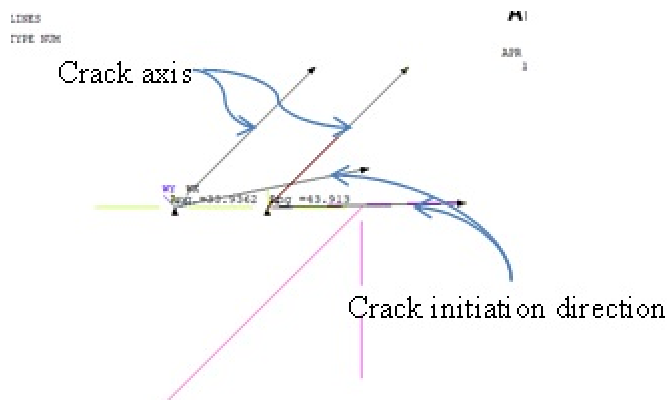

Fig 7 Vector direction of a node having maximum first principal stress for crack inclined at 45° to the loading axis

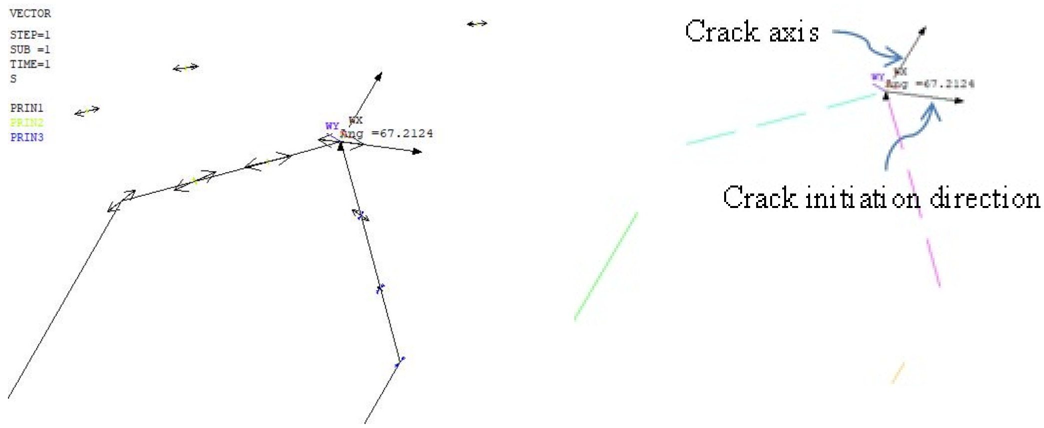

(a) (b)

Fig 8 (a) Vector direction of various nodes at and around the crack tip along with (b) Vector direction of a node having maximum first principal stress for crack inclined at 60° to the loading axis

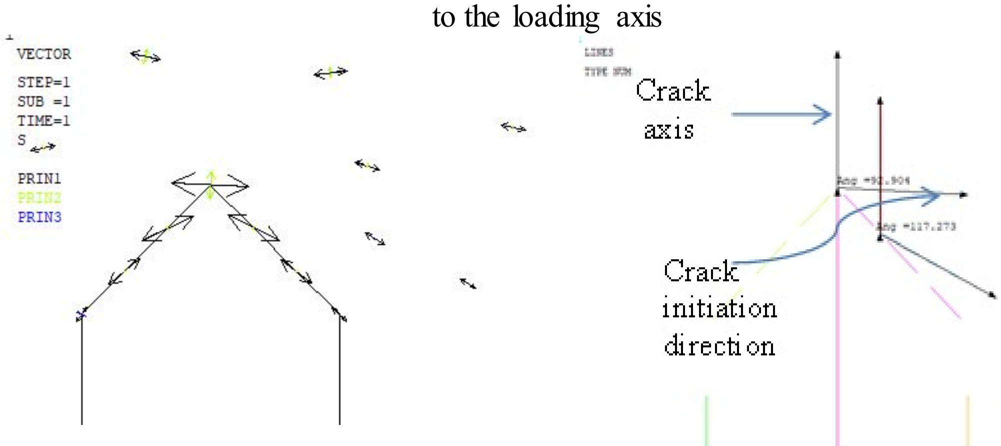

(a) (b)

Fig 9 (a) Vector direction of various nodes at and around the crack tip along with (b) Vector direction of a node having maximum first principal stress for crack inclined at 90° to the loading axis

Table below compares the vector directions of a node of maximum principal stress (i.e. crack initiation angle) obtained from the simulation for various crack inclinations, to the critical polar angles of the plastic zone curves obtained from formulations.

Crack inclination (in degree)	Crack initiation angles(in degree) obtained from simulation	Range of Dip Angles/Critical polar angles (in degree) of plastic zone curves for various Poisson's ratio
0	5	0
30	-45	-24 to -30
45	-39	-40 to -47
60	-67	-85 to -93
90	-92	-99

APPENDIX E

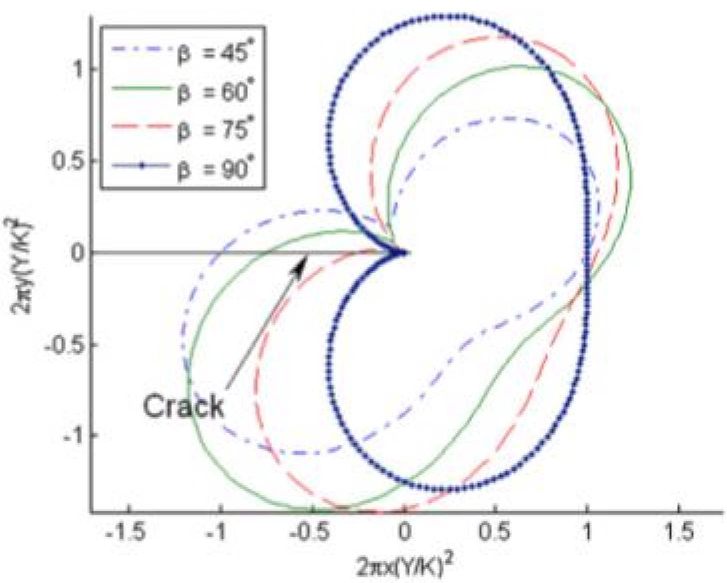

Fig 1 Numerical simulation of plastic zone shapes for mixed mode I/II crack under uniaxial loading for isotropic materials (Xin G. et al., 2010[43])

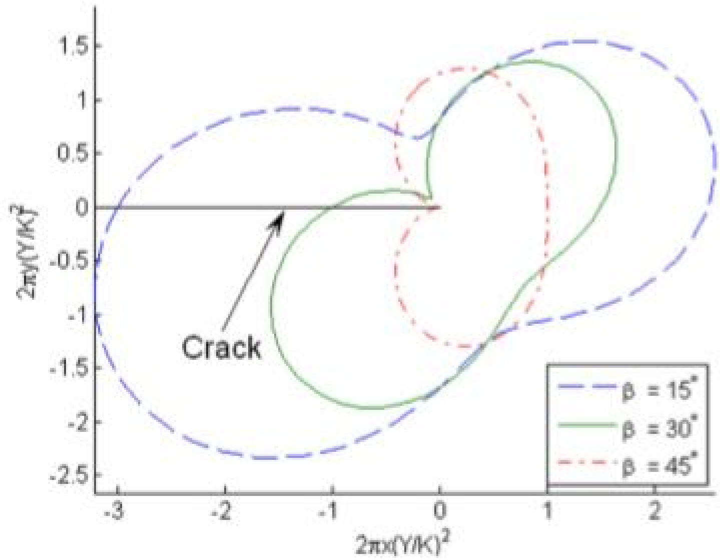

Fig 2 Numerical simulation of plastic zone shapes for mixed mode I/II crack under pure shear loading for isotropic materials (Xin G. et al., 2010[43])

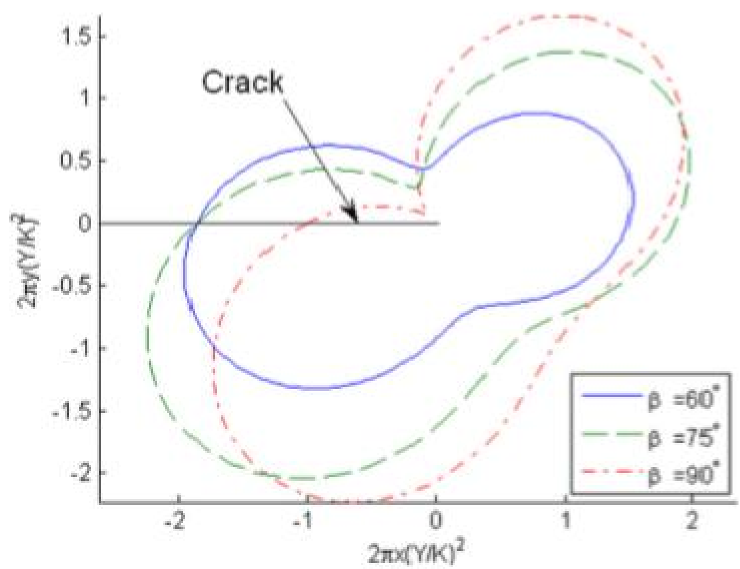

Fig 3 Numerical simulation of plastic zone shapes for mixed mode I/II crack under proportional tension shear loading for isotropic materials (Xin G. et al., 2010[43])

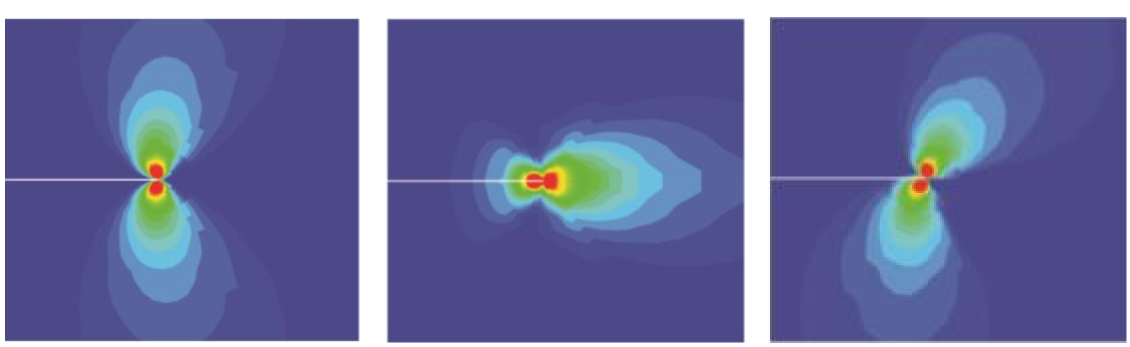

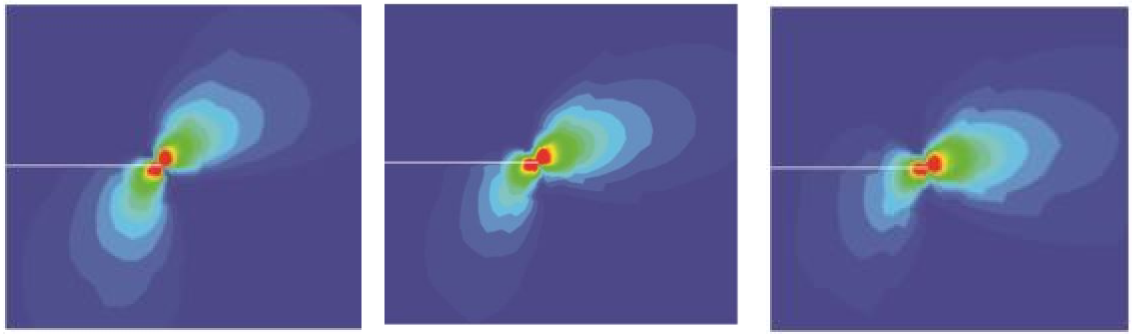

Fig 4 Numerical simulation of plastic zone shapes for Pure mode I, II and mixed mode I/II for Pseudo-elastic shape memory alloy (Ardakani S.H. et al., 2016[44])